DOI: 10.11858/gywlxb.20230783

Prediction of Synthesis Condition and Magnetic Property of Screened Metallic Double-Perovskite Antiferromagnet Mn_2FeOsO_6

LI Jun[1], JIN Shangjian[2], ZHAO Shuang[3], YAO Daoxin[2], LI Manrong[3,4]

（1. *Key Laboratory for Microstructural Material Physics of Hebei Province*, *School of Science*, *Yanshan University*, *Qinhuangdao* 066004, *Hebei*, *China*;
2. *State Key Laboratory of Optoelectronic Materials and Technologies*, *School of Physics*, *Sun Yat-sen University*, *Guangzhou* 510275, *Guangdong*, *China*;
3. *Key Laboratory of Bioinorganic and Synthetic Chemistry of Ministry of Education*, *School of Chemistry*, *Sun Yat-sen University*, *Guangzhou* 510275, *Guangdong*, *China*;
4. *School of Science*, *Hainan University*, *Haikou* 570228, *Hainan*, *China*）

Abstract: We present a theoretical approach for predicting the electron configuration, polymorph, synthesis condition, and physical properties of complex magnetic double perovskite compounds. Our method is reasonable and computationally efficient, allowing us to identify an antiferromagnetic (AFM) metallic material, namely Mn_2FeOsO_6, with a high AFM Néel transition temperature (T_N). Through extensive analysis, we demonstrate that Mn_2FeOsO_6 possesses a high density of states near the Fermi level and an AFM configuration, resulting in a zero total magnetic moment. Our findings suggest that the expected T_N of Mn_2FeOsO_6 is as high as 680 K, representing a potential breakthrough in the field of spintronics. We have also constructed a sophisticated magnetic model for this material, and obtained a reasonably reliable magnetic excitation spectrum potentially comparable with neutron scattering spectra. This theoretical approach provides synthesis conditions that are consistent with many synthesized double perovskite compounds in experiments, and it holds promise for the prediction of other complex magnetic configurations. Our study may play a key role in the big data prediction of novel double perovskite materials.

Keywords: double-perovskite；antiferromagnet；Mn_2FeOsO_6

CLC number: O521.2 **Document code:** A

* **Received date:** 2023-11-08；**Revised date:** 2023-12-25

Foundation item: National Natural Science Foundation of China (22090041, 11974432, 92165204); National Key Research and Development Program of China (2018YFA0306001, 2022YFA1402802); Guangdong Basic and Applied Basic Research Foundation (2019A1515011337); Natural Science Foundation of Hebei Province (A2021203010); Leading Talent Program of Guangdong Special Projects (201626003); International Quantum Academy of Shenzhen (SIQSE202102); Program for Guangdong Introducing Innovative and Entrepreneurial Teams (2017ZT07C069)

Biography: LI Jun (1987—), male, lecturer, primarily engaged in research related to computational physics simulations. E-mail: ljcj007@ysu.edu.cn

Corresponding author: YAO Daoxin (1973—), male, professor, primarily engaged in research on condensed matter theory. E-mail: yaodaox@mail.sysu.edu.cn
LI Manrong (1977—), male, professor, primarily engaged in research on the physics and chemistry of materials under extreme conditions. E-mail: limanrong@mail.sysu.edu.cn

The field of antiferromagnetic (AFM) spintronics has recently garnered attention due to its ultrafast dynamics, zero net magnetization, and stability against external magnetic fields, which hold promise for future computing power[1–4]. In these materials, information can be encoded by manipulating the antiferromagnetic order via domain wall motion[5], optical excitation[6], spin-orbit torques[3], and staggered local relativistic fields[7]. Among the different categories of antiferromagnet, metallic antiferromagnet are particularly unique as they provide an ideal platform for fundamental studies and applications due to the strong interplay between electrons, spin, phonons, and photons[8–9]. However, metallic antiferromagnets are rare, and the known materials display AFM order only well below room temperature (RT), which limits their practical applications. For instance, the transition-metal oxides $Nb_{12}O_{29}$[10], $Ca_3Ru_2O_7$[11], $CaCrO_3$[12], and $LaNiO_3$[13] exhibit Néel transition temperature T_N of 12, 56, 90, and 157 K, respectively. Although RuO_2 exhibits AFM order at around RT (T_N ~ 300 K), the magnetic moment is as small as $0.05\mu_B$ (μ_B represents Bohr magneton) at about 300 K. Therefore, exploring materials with RT magnetic order is of utmost importance for practical magnetic applications[1].

Recently, research on the magnetic properties of double-perovskite oxides $A_2BB'O_6$, where B and B′ are ordered 3*d* and 4*d*/5*d* transition metal ions, has demonstrated the emergence of homogeneous and long-range magnetic order due to periodic intrinsic magnetic ions and magnetic exchange interactions[2–9]. These materials exhibit multiple functions resulting from multiple physical interactions, such as spin, orbit, dipole, and lattice. For example, such interactions give rise to magnetoelectric coupling based multiferroics[14–15], half-metallicity[16], colossal magnetoresistance[16], and ferromagnetic (FM) semiconductor and insulator[17] properties in RT perovskite-oxides magnets.

Theoretical analysis of $A_2BB'O_6$ materials with divalent A-site alkali earth cations reveals that the maximum number of unpaired 3*d* and 4*d*/5*d* electrons can reach $3d^5$ ($t_{2g}^3e_g^2$ in high spin) or $4d^3/5d^3$ ($t_{2g}^3e_g^0$) combination over the B- and B′-sites, such as in $A_2Fe^{3+}B'^{5+}O_6$ (B′ = Ru, Os) and $A_2Mn^{2+}B'^{6+}O_6$ (B′ = Rh, Ir) under charge balance. For example, the Ca_2FeOsO_6 material exhibits electrically insulated behavior and undergoes a FM transition at about 320 K driven by lattice distortion and chemical pressure[6, 18–19]. In contrast, spin frustration arising from the disordered alignment of Fe^{3+}/Ru^{5+} in A_2FeRuO_6 (*Pbnm* symmetry)[20–21] may result in spin-glass or AFM behavior[22]. Notably, the Fe/Ru ordered double perovskite Sr_2FeRuO_6 is stabilized in film form by hetero-interface strain (chemical pressure) on $SrTiO_3$ substrate, achieving a Curie temperature (T_C) of 390 K[23]. To date, there are no reports on $A_2Mn^{2+}Rh^{6+}O_6$ or $A_2Mn^{2+}Ir^{6+}O_6$.

The emerging research on exotic perovskites under high-pressure and high-temperature (HPHT) conditions has led to the investigation of transition metal cations at the A-site, resulting in enhanced magnetic interactions when compared to conventional analogs[14–15, 17, 24–34]. The occupancy of the A-site by high-spin d^5-Mn^{2+} cations can significantly increase the number of unpaired d electrons, thereby promoting strong magnetic interactions in $Mn_2BB'O_6$[35]. Theoretically, there are 411 possible combinations of $Mn_2BB'O_6$ in $Mn_2B^{1+}B'^{7+}O_6$, $Mn_2B^{2+}B'^{6+}O_6$, and $Mn_2B^{3+}B'^{5+}O_6$, as shown in Fig. 1. $Mn_2B^{4+}B'^{4+}O_6$ is unlikely to form ordered double perovskites and is ignored here. Up to now, only 20 compounds have been experimentally validated to crystallize in Mg_3TeO_6-type ($R\bar{3}$)[36–37], Ni_3TeO_6-type ($R3$)[38–39], β-Li_3VF_6-type ($C2/c$)[40–42], and $GdFeO_3$-type ($P2_1/n$)-type[43–44] structures, depending on the chemical and synthesis parameters (see Fig. 1).

Taking the number of unpaired d electrons (n_d), chemical valences and ionic radius into account, it is noteworthy that eight transition-metal-only (TMO) double perovskites with n_d between 14 and 18 exhibit robust magnetoelectric properties, which provides motivation for further exploration in this category. More than 70 TMO double perovskites can be formed in $Mn_2BB'O_6$ by ordered combination of 3*d* and 4*d*/5*d* ions over B- and B′-sites under charge balance, offering a vast space to explore new multifunctional materials. However, the normally arranged atoms will have a certain displacement and deformation due to the influence of strong magnetism[45],

making TMO double perovskites' symmetry further reduced than that of conventional nonmagnetic perovskites. As a result, tolerance factor (t)[46–47] and octahedral factor (μ)[48–49] as geometric descriptors for conventional perovskites with large A-cations are not longer suitable for the TMO double perovskites. Therefore, discovering these materials mainly relies on empirical intuition and costly trial-and-error in HPHT synthesis.

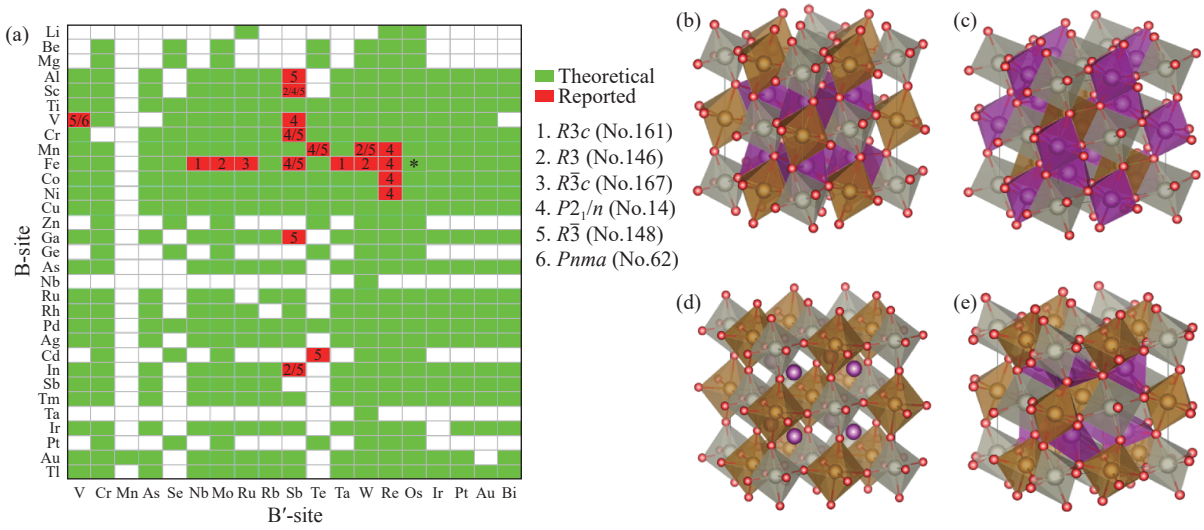


Fig. 1　(a) Possible combinations of $Mn_2BB'O_6$ in the chemical space of B and B′ cations under charge balance (The possible, reported, and inexistent compounds are displayed in green, red, and blank, respectively. The numbers marked for the 20 known compounds denote the space group types listed on the right side.); (b)–(e) the crystal structures of some of the known compounds, including Mg_3TeO_6-type ($R\bar{3}$)[36–37], Ni_3TeO_6-type ($R3$)[38–39], β-Li_3VF_6-type ($C2/c$)[40–42], and $GdFeO_3$-type ($P2_1/n$)[43–44] (To ensure that our calculations are compatible with different magnetic configurations and atomic distortions, we have used a 40-atom super-cell, which can be considered as a (2, 2, 2) multiple of the ideal single perovskite structure along the three axes of Cartesian coordinates[50–51]. (b)–(e) also show the examples of collinear magnetic structure that we considered structure optimization with (b) FM, (c) Type Ⅰ AFM, (d) Type Ⅱ AFM and (e) Type Ⅲ AFM.)

Recently, the successful prediction and precise synthesis of A_3TeO_6 have provided insight into the screening of new materials oriented towards structure and function, which can help avoid the costly trial-and-error process involved in preparing magnetically exotic perovskites under HPHT[52–53]. These studies have used first-principles density functional theory (DFT) calculations based on the Murnaghan equation of state for solids[54] to show that the phase stability between competing polymorphs can be estimated using the phase diagram of the relative enthalpy (ΔH), the total energy (E) and the pressure (p). The reported DFT-based workflow, which adopts a restricted collinear magnetic structure, has been shown to provide considerable accuracy in predicting the polymorph and corresponding synthesis parameters (such as pressure). However, for TMO double perovskites with 4*d*/5*d* ions at the B′-site, the variation in the energy scale of possible interactions, such as magnetic interactions, spin-orbit coupling (SOC), Dzyaloshinskii-Moriya (DM) interaction, Hubbard U and Hund's interactions, cause a challenge for calculating these materials reliably and efficiently using *ab initio* many-body methods[45]. This remains an open challenge in providing reliable and timely predictions for this strongly correlated perovskites family[55–56]. Conversely, validation calculations based on experimentally reported TMO double perovskite-related compounds are expected to facilitate the understanding of dominant factors in inverse prediction and rational design.

In this article, we will firstly conduct test calculations on the known transition metal oxide $Mn_2BB'O_6$, establish calculation models, and then these models will be used to predict the pressure-dependent polymorph evolution and synthesis parameters of the TMO double perovskite Mn_2FeOsO_6, which contains a maximum n_d of

18. Additionally, we will propose several magnetoelectric properties of Mn_2FeOsO_6. Due to the high cationic disordering in corundum-type, Mn_2FeRuO_6 is beyond the scope of this work, shown experimentally[25].

1 Symmetry Analysis

For double perovskite materials with the chemical formula $A_2BB'O_6$, the ideal crystal structure is usually doubled in all three crystallographic directions compared to a single perovskite ABO_3, resulting in a space group of $Fm\bar{3}m$[32]. However, this only occurs when the size of the A-site cation is much larger than that of the B-site cation, i. e. with tolerance factor t around 1[57]. When the size of the A-site cation is comparable to that of the B-site cation, i. e. with tolerance factor t less than or equal to 0.85, the BO_6 octahedra will tilt to optimize the A-cation bonding[58]. According to Glazer's tilt rule, there can be 12 tilt systems in $A_2BB'O_6$ perovskites, as determined by Howard *et al*[59−60]. As mentioned in our previous article[53], exotic double perovskites with transition metals and $t\leqslant 0.85$ may adopt one of six possible structures identified by database screening, including distorted $GdFeO_3$-type double perovskite ($P2_1/n$), B-site ordered $LiSbO_3$ derivatives ($Pnn2$), Mg_3TeO_6 ($R\bar{3}$)[36−37], corundum derivatives ($LiNbO_3$-type $R3c$, ilmenite $R\bar{3}$, and ordered ilmenite or Ni_3TeO_6-type $R3$)[38−39], bixbyite ($Ia\bar{3}$), and β-Li_3VF_6 ($C2/c$)[40−42]. Based on chemical and geometrical considerations, the size and the charge differences between the A-site and B-site cations studied in this paper do not energetically favor the formation of bixbyite ($Ia\bar{3}$) and $LiSbO_3$ derivatives ($Pnn2$). Therefore, we only consider the remaining four structures ($R3$, $R\bar{3}$, $C2/c$ and $P2_1/n$).

Stretching the ideal face-centered cubic structure $Fm\bar{3}m$ along the <111> direction results in the $R\bar{3}$ structure, where the BO_6 octahedra tilts and the space group changes to $a^-a^-a^-$ in Glazer tilt systems. However, in practice, the orders of B and B′ coordination can destroy the space-reversal symmetry, leading to the $R3$ polymorphs. The reported $R3c$ structure is unlikely to happen for rock-salt double perovskite structures.

Meanwhile, the $C2/c$ and $P2_1/n$ structures can be obtained by sliding the ideal $Fm\bar{3}m$ structure along the <110> direction and considering the tilt of the BO_6 octahedra. In the case of small A-cations, the A cation is unlikely to maintain the ideal position, leading to the distortion of the lattice and the formation of the $P2_1/n$ structure with $a^+b^-b^-$ in Glazer tilt systems. Both $C2/c$ and $P2_1/n$ configurations are commonly observed in double perovskite structures.

The single perovskite structure is also the most abundant in $Pnma$ ($a^+b^-b^-$) and $R\bar{3}c$ ($a^0b^-b^-$) configurations[48, 61] since the tilt direction of BO_6 octahedra in the adjacent two layers of perovskite structure tends to be opposite. In the Glazer symbol, therefore, compared with in-phase BO_6 rotations, such as $Im\bar{3}$ ($a^+a^+a^+$) and $Pmmn$ ($a^-b^+b^+$), the anti-phase BO_6 rotations are more common. When it comes to double perovskites $A_2BB'O_6$, two typical progress of octahedral tilts with decreasing t has been found as[62−63]

$$\begin{aligned} &Fm\bar{3}m\left(a^0a^0a^0\right)\rightarrow R\bar{3}\left(a^-a^-a^-\right)\rightarrow R3\left(a^-a^-a^-\right)\\ &Fm\bar{3}m\left(a^0a^0a^0\right)\rightarrow C2/c\left(a^0b^-b^-\right)\rightarrow P2_1/n\left(a^+b^-b^-\right)\end{aligned} \tag{1}$$

We note that in material calculations, A-site cations are always repelled or attracted by B-site cations due to the influence of magnetism and Jahn-Teller effect, making it difficult to maintain a square arrangement in a plane. Therefore, the common tetragonal lattice ($I4/m$ ($a^0a^0c^-$) or $P4/mnc$ ($a^0a^0c^+$)) in perovskite is hard to appear under the condition that both A- and B-sites of double-perovskite are transition metal ions. In fact, experimental research on this type of materials has also confirmed our conclusion, i. e. there is no report on tetragonal lattice double-perovskite oxides with A-site alkali earth cations, B and B′ ordered transition metal ions so far, as shown in Fig. 1(a).

In this work, we investigated the effect of magnetism on the lattice distortion of double perovskite structures,

in addition to the BO_6 octahedral tilt induced by the small A-cation. Previous studies have also reported the influence of magnetism on the lattice distortion phenomenon[22–23, 45]. It is important to note that the nearest-neighbor (NN) and next nearest-neighbor (NNN) interactions can have similar strengths. In the ideal double perovskite structure, there are many possible magnetic configurations. However, experimental observations have shown that only four magnetic configurations are mostly observed. There are three types of AFM order, namely, type-Ⅰ, type-Ⅱ, and type-Ⅲ, depending on the relative magnitudes of NN and NNN interactions. For type-Ⅰ order, the spins are anti-parallel between the [100] planes and parallel within the [100] plane. Type Ⅱ order occurs when the NN interactions are weaker than the NNN interactions, with the spins arranged anti-parallel between the [111] planes and parallel within the [111] plane. Type-Ⅲ order is an intermediate form in which the NN interactions are relatively strong, while the NNN interactions are still significant.

In addition to these four configurations, there are other disordered magnetic phases such as magnetic frustration and spin-glass-type behavior. However, these phases are less relevant to the present study, therefore, we limit our DFT calculation and analysis of structural optimization to the four aforementioned configurations. When analyzing the magnetic properties of materials, we consider as many magnetic configurations as possible to obtain more reliable magnetic properties.

Since most experimental synthesis of transition-metal double perovskites require HPHT conditions[64–66], we considered the synthesis pressure as a crucial parameter. To investigate the effect of pressure on the stability of double perovskite structures, we calculated the energies of all four lattice configurations and four magnetic configurations for each material under varying pressure conditions.

2　Model and Methods

To simulate the application of relatively large pressure, we started with a relatively small initial volume for each polymorph with a specific set of ingredients. We then gradually increased the simulating pressure by reducing the lattice to determine the most stable structure type at each given pressure. After that, we obtained the total energy (E) and volume (V) curve of each compound, and fit it with the Brich-Murnaghan function

$$E(V) = -\frac{9}{16}B_0\left[(4-B_0')\frac{V_0^3}{V^2} - (14-3B_0')\frac{V_0^{7/3}}{V^{4/3}} + (16-3B_0')\frac{V_0^{5/3}}{V^{2/3}}\right] + E_0 \tag{2}$$

where B_0, B_0', V_0 and E_0 are fitting parameters. We finally obtained the relative energy-pressure (E-p) relation to determine the phase transition of each compound

$$p(V) = 1.5B_0\left[\left(\frac{V_0}{V}\right)^{7/3} - \left(\frac{V_0}{V}\right)^{5/3}\right] \tag{3}$$

Our DFT calculations were performed using the Vienna *ab initio* simulation package (VASP)[67–70] with the projector augmented wave (PAW) method. We used the spin-polarized generalized gradient approximation (GGA) and the Perdew Burke-Ernzerhof (PBE) function to treat the electron exchange correlation potential[71]. The plane wave kinetic energy cutoff was set to 400 eV.

To ensure our calculations are compatible with different magnetic configurations and atomic distortions, we used a 40-atom supercell, which can be considered as a (2, 2, 2) multiple of the ideal single perovskite structure along the three axes of Cartesian coordinate[50–51]. The Γ point only in VASP was used to accelerate the crystal structure optimization until the force on each atom is less than 0.001 eV/Å. We built initial structure models for calculations by elemental substitutions of the crystallographic information files of known compounds with elemental substitutions.

To investigate the effect of pressure on the stability of double perovskite structures, we applied isotropic pressure during the calculations. In DFT calculations, we have considered various factors, such as collinear

magnetic structure, SOC, DFT+U (U_{Fe} = 4.6 eV, U_{Mn} = 4 eV, U_{Os} = 2.0 eV), and non-collinear magnetic structure to determine which factors would have undeniable impact on the structure.

For Mn_2FeOsO_6, its magnetic properties can be described by the Heisenberg Hamiltonian

$$H = -\sum_{i,j} J_{ij}\boldsymbol{S}_i\cdot\boldsymbol{S}_j - \boldsymbol{D}(\boldsymbol{S}_i\times\boldsymbol{S}_j) - \sum_i \Delta_s(\boldsymbol{S}_i^z)^2 \tag{4}$$

where the symbol $\boldsymbol{S}_i$ ($\boldsymbol{S}_i^z$) represents the spin operator at the lattice site i (along the z direction), J_{ij} refers to the Heisenberg exchange between $\boldsymbol{S}_i$ and $\boldsymbol{S}_j$, $\boldsymbol{D}$ refers to the DM interaction, and Δ_s represents the single-ion Ising anisotropy.

There are 8 magnetic atoms in a supercell, and it is needed to consider 64 types of magnetic exchange interactions between these magnetic ions. If we ignore magnetic exchange interaction J between identical magnetic ions (i. e. J_{ii} = 0) and the directional dependence between different magnetic ions (i. e. $J_{ij} = J_{ji}$), there are 28 distinct values left. Therefore, we need to calculate these 28 different magnetic exchange interaction values individually.

We calculated 64 different magnetic configurations among the total 2^8 = 256 configurations in the magnetic unit cell containing 8 magnetic ions. Because the magnetic anisotropy is basically negligible, we used collinear magnetic DFT calculations to save the resources requirement. These 64 magnetic configurations are enough to obtain 28 unknown J. In order to simplify the calculation, we used the linear matrix method to calculate J one by one using the minimum dichotomy method

$$\tilde{\boldsymbol{J}} = \tilde{\boldsymbol{E}}/(\tilde{\boldsymbol{S}}\otimes\tilde{\boldsymbol{S}}) \tag{5}$$

where $\tilde{\boldsymbol{J}}$ is a 1×28 matrix contained 28 different magnetic exchange interaction values, $\tilde{\boldsymbol{E}}$ is a 64×1 matrix contained 64 different energies obtained by DFT calculations, and $\tilde{\boldsymbol{S}}\otimes\tilde{\boldsymbol{S}}$ represents the direct product between magnetic moments of the magnetic ions.

To study the spin dynamic behaviours, we applied a linear spin wave theory by using SpinW package to compute the excitation spectrum[72]

$$I(k,\omega) \propto \sum_{\alpha,\beta}\left(\delta_{\alpha,\beta} - \tilde{k}_\alpha\tilde{k}_\beta\right)S^{\alpha,\beta}(k,\omega) \tag{6}$$

where k is normalized wave vector, ω is frequency of the excitation spectrum, $S^{\alpha,\beta}$ ($\alpha, \beta = x, y, z$) is the dynamic structure factor, $\tilde{k}_\alpha$, $\tilde{k}_\beta$ are components of the normalized wave vector k, $\delta_{\alpha,\beta}$ is the Dirac delta function which takes the value of 1 only when $\alpha=\beta$, otherwise it takes 0.

3　Validation Calculations on Known Two Double Perovskites

Table 1 provides the details of the synthesis conditions, structural symmetry, electron configurations, and physical properties of TMO double perovskites $A_2BB'O_6$ where B- and B′-site cations is transition-metal atoms. The Re-based compounds crystallize in a distorted $GdFeO_3$-type monoclinic structure ($P2_1/n$), while Mo-based and W-based compounds are more likely to adopt rhombohedral symmetry ($R3$). Previous studies have shown that DFT caculations in consideration of only collinear magnetic structures can yield reasonable and acceptable overall trends of synthesis condition and E-p phase diagrams for TMO double perovskites[52−53].

We investigated the effect of other possible properties, such as DFT+U (U_{Fe} = 4.6 eV, U_{Mn} = 4 eV, U_{Os} = 2.0 eV), and the role of non-collinear magnetic structure, on the energy-volume (E-V) results, but found that these interactions do not impact the results significantly. Therefore, we concluded that these additional interactions could be ignored in structural optimization, and we only adopted collinear magnetic structures in the structural optimization calculations to save computational resources.

Table 1　Structural and electronic properties of the 7 experimentally realized TMO double perovskite-related compounds, along with the predicted Mn_2FeOsO_6. Here $n_d \geqslant 14$ provide certain displacement and deformation due to the influence of strong magnetism, resulting in low symmetry (*R*3 and $P2_1/n$)

Compound	Space group	n_d	Synthesis conditions	Physical properties	Magnetic structure	Ref.
Mn_2FeMoO_6	*R*3	16	1 350 ℃, 8 GPa	Multiferroic, T_C = 337 K	Type-Ⅱ AFM	[17]
Mn_2FeWO_6	*R*3	14	1 400 ℃, 8 GPa	Second-Harmonic generation, T_N = 70 K	Type-Ⅰ AFM	[24]
Mn_2MnWO_6	*R*3	15	1 400 ℃, 8 GPa	T_N = 58 K	Type-Ⅰ AFM	[15]
Mn_2CoReO_6	$P2_1/n$	14	1 300 ℃, 8 GPa	Semiconductor, T_N = 94 K	Type-Ⅱ AFM	[26]
Mn_2FeReO_6	$P2_1/n$	17	1 350 ℃, 5/11 GPa	Half-metal, T_C = 520 K	Type-Ⅲ AFM	[16, 29–30]
Mn_2MnReO_6	$P2_1/n$	17	1 400 ℃, 5/8 GPa	Semiconductor, T_N = 50 K	Type-Ⅱ AFM	[29, 31]
Mn_2NiReO_6	$P2_1/n$	17	1 573 ℃, 8 GPa	Semiconductor, T_N = 80 K	Type-Ⅱ AFM	[73]
Mn_2FeOsO_6	$P2_1/n$	18	5 GPa	Metal, T_N = 680 K	Type-Ⅲ AFM	This work

To be clear, we started with Mn_2MnReO_6 with the known $P2_1/n$ structure synthesized in previous studies[16, 29–30]. To evaluate the effect of magnetism on the crystal structure, we calculated the *E*-*V* curve using the Brich-Murnaghan function. It turns out that for collinear magnetic structures, the magnetism contribution to the energy difference is on the order of 0.1 eV/atom, accordingly, having an effect on the lattice structure. However, the *E*-*p* curve calculated using Eq. (3) shows that, the *R*3 structure is the most stable one when $p \leqslant 10$ GPa, with a minimum energy difference of less than 0.1 eV per cell without considering the magnetic structure. This small energy difference results in inconsistency between the calculated *R*3 output and the experimental $P2_1/n$ result. Therefore, we must consider the magnetic structure in TMO double perovskites. We conjectured that the magnetic exchange between magnetic ions in Mn_2MnReO_6 would affect the crystal structure, and the magnetic contribution of atoms should be considered in the DFT calculations of structure optimization. After considering magnetic structure, the type-Ⅱ AFM configuration has the lowest energy of the four collinear magnetic structures considered, which is a good validation of previous experiment results[29–31].

In the present study, we investigated the polymorphic phase transitions of five double perovskite compounds, namely Mn_2MnReO_6, Mn_2CoReO_6, Mn_2FeReO_6, Mn_2FeMoO_6, and Mn_2FeWO_6. In our calculations, we have considered the four different magnetic configurations and obtained their respective *E*-*V* relations (see Fig. 2(a)–Fig.2(e)). However, due to the existence of metastable magnetic structures, the total magnetic moment after DFT convergence is found to be inconsistent with the calculations of a single magnetic configuration. The *E*-*V* curves also exhibit abnormal points and protrusions, rendering the fitting of these curves with the Brich-Murnaghan function inaccurate. To address this issue, we selected the magnetic structure with the lowest energy under each *V* point of the four magnetic configurations as the source of *E*-*V* curve. By uniformly fitting these *E*-*V* curves with the lowest energy, we obtained appropriate parameters to produce a sufficiently reliable *E*-*p* curve.

Upon adding magnetism, we observed that although the influence of magnetism on each structure is different, the total energy of the system is reduced by about 1 eV per cell. For Mn_2MnReO_6, such a small influence of magnetic exchange energy is able to reverse the two energy levels of *R*3 and $P2_1/n$ structures under the external pressure around 7 GPa, beyond which the $P2_1/n$ structure is more stable and in good agreement with the experimental results[29, 31]. Notably, 5 GPa is needed to prepare $P2_1/n$ Mn_2MnReO_6 in the experiment[29], and the gap of 2 GPa between theory and experiment may be caused by the 1 400 ℃ treatment and can be considered as within the theoretical error range.

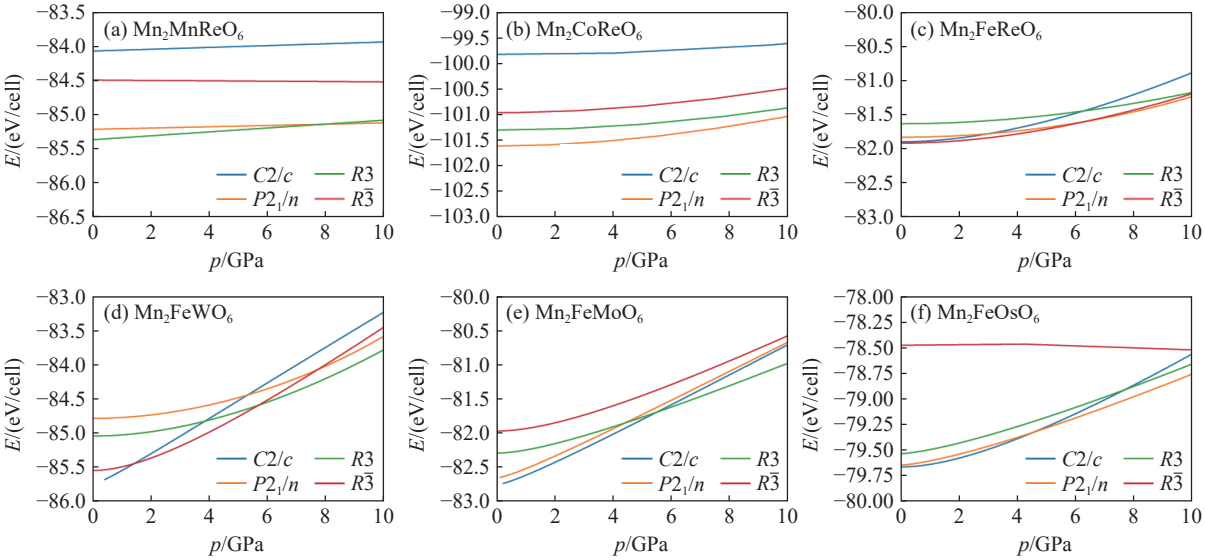


Fig. 2　*E*-*p* curves of Mn_2FeWO_6 and Mn_2FeMoO_6, as well as Mn_2FeOsO_6 with the magnetic structures in Table 1. (All these results are fitted by Brich-Murnaghan function Eq. (3) in consideration of the lowest energy of four collinear magnetic configurations.)

We then applied this method to the related double perovskite compounds that had been experimentally prepared. In our calculations, the lowest synthesis energy configuration of Mn_2CoReO_6 is always the $P2_1/n$ structure, which roughly echoes the experimental results[26]. For Mn_2FeReO_6, the synthesis energies of the four structures exhibit little differences in the pressure range considered. The energy of $R\bar{3}$ overlaps that of $P2_1/n$ at 5 GPa, being consistent with the synthetic conditions in the experiment[16]. The situations of Mn_2FeMoO_6 and Mn_2FeWO_6 are similar. Both compounds show the $R3$ structure under high pressure, and the synthesis conditions are about 6 GPa. We also checked the calculations without considering magnetic conditions and found that they do not match experiments. Validation calculations on these five synthesized double perovskite materials prove that our proposed method for computing polymorph-dependent phase diagrams is reliable.

4　Magnetism of Mn_2FeOsO_6

In this section, we present predictions on the structure and the properties of Mn_2FeOsO_6, a compound that has not yet been experimentally synthesized. Our DFT calculations demonstrate that the $C2/c$ structure is relatively stable under atmospheric pressure, as illustrated in Fig. 2(f). However, under a pressure greater than 5 GPa, the $P2_1/n$ structure with type-Ⅲ AFM configuration becomes the most stable.

In addition, our calculations on the possible magnetic structures of Mn_2FeOsO_6 revealed a standard AFM configuration, where the magnetism of each magnetic ion is reversed. Specifically, in a 40-atom supercell, four spins of the eight Mn atoms are opposite to the other four, and two spins of the four Fe atoms are also opposite to the other two. We have also confirmed that the magnetic anisotropy is relatively small, as the energy difference per cell caused by magnetism in the lattice vectors *a*, *b*, and *c* (Fig. 3(a)) directions is less than 0.1 meV.

We then proceeded to approximate the magnetic properties of Mn_2FeOsO_6. Our calculations showed that the total magnetic anisotropy energy (MAE) in a single magnetic unit cell is negligible (Δ_s<0.1 meV) in consideration of SOC, and the spins of magnetic atoms exhibit almost collinear configuration with only a degree difference of less than 5°, as depicted in Fig. 3(a). Therefore, in the estimation of magnetic properties, we neglected the MAE, as well as DM interaction, and only considered Heisenberg exchange in Eq. (4).

As illustrated in Fig. 3, Mn_2FeOsO_6 contains 8 magnetic ions in a single magnetic unit cell. Among them, the four Mn ions possess a local magnetic moment of approximately 4.5μ_B, and the two Fe ions possess a local

magnetic moment of approximately $4\mu_B$, while the two Os ions possess a local magnetic moment of approximately $1\mu_B$. Although basically Os ions is not magnetic, they exhibit magnetism induced by the surrounding strong magnetic Mn and Fe ions.

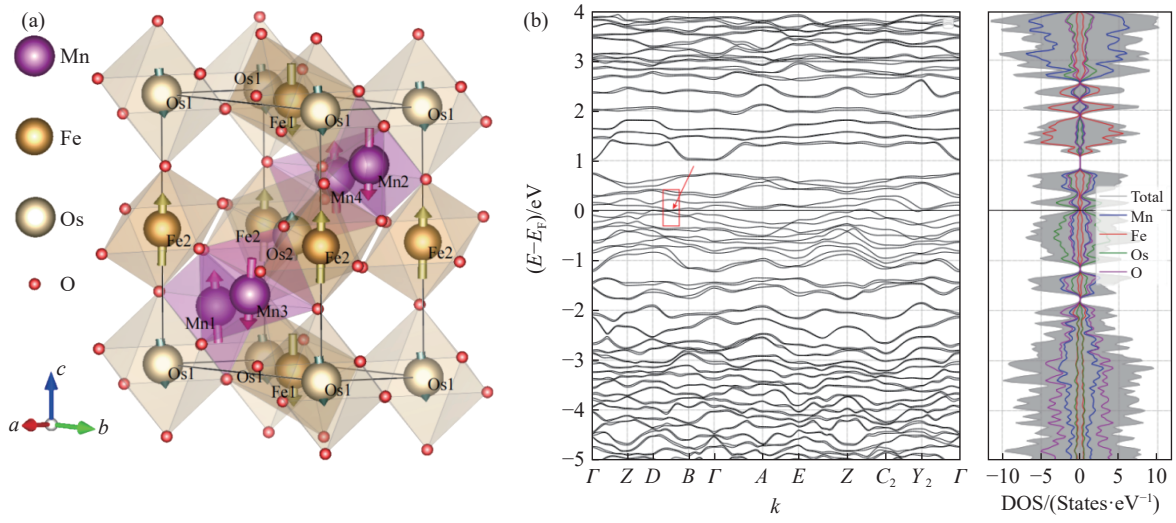


Fig. 3　DFT results of Mn_2FeOsO_6 in consideration of SOC, DFT+U (U_{Fe} = 4.6 eV, U_{Mn} = 4 eV, U_{Os} = 2.0 eV) and non-collinear magnetism: (a) the predicted atomic and magnetic structures, with a distorted $GdFeO_3$-type monoclinic structure ($P2_1/n$) as for Mn_2FeReO_6[16, 29–30] (The arrow on each atom represents the spin orientation and the size of spin value. Every spin is almost laying at <001> direction, forming a relatively ideal AFM configuration.); (b) energy band structure near Fermi level and spin-resolved density of states (DOS) (Mn_2FeOsO_6 has no bandgap, forming as conductor. There is a suspected formation of Dirac points between wavevectors *B*-*D*, marked by red rectangle and arrow. The DOS of spin-up and spin-down are basically the same, verifying the AFM configuration of Mn_2FeOsO_6.)

In our magnetic exchange model for Mn_2FeOsO_6, we calculated 28 different J due to the irregular configuration of the magnetic ions in the $P2_1/n$ structure. Here, we present a few examples to illustrate the numerical values of these J . The AFM exchanges ($J > 0$) between the NN Mn ions ($J_{13} \approx J_{24}$) and NNN ones are approximately equal to the values reported in [74]. However, due to the low symmetry of $P2_1/n$, there are two different distances between NN Mn ions, resulting in slightly different FM exchanges ($J_{23} < J_{14}$) induced by indirect Ruderman-Kittel-Kasuya-Yosida (RKKY) exchanges. Thus, our group of magnetic exchange models, which contains 8 different magnetic ions, is considered to be reliable.

According to the aforementioned magnetic structure model, we constructed the corresponding exchange interactions between magnetic ions, as shown in Table 2. The result of spin dynamic behaviours of Mn_2FeOsO_6 is shown in Fig. 4(b). Note that we have ignored the DM interaction and single-ion Ising MAE in the Hamiltonian.

Table 2　Magnetic exchange J_{ij} between magnetic ions within a magnetic unit cell of Mn_2FeOsO_6

i	j	J_{ij}/meV	i	j	J_{ij}/meV	i	j	J_{ij}/meV	i	j	J_{ij}/meV
Mn1	Mn2	0.97	Mn2	Mn3	−19.20	Mn3	Fe1	1.01	Mn4	Os2	−15.77
Mn1	Mn3	40.48	Mn2	Mn4	39.88	Mn3	Fe2	13.49	Fe1	Fe2	−12.01
Mn1	Mn4	−20.07	Mn2	Fe1	15.06	Mn3	Os1	−16.74	Fe1	Os1	35.37
Mn1	Fe1	−14.33	Mn2	Fe2	18.32	Mn3	Os2	15.65	Fe1	Os2	35.37
Mn1	Fe2	−16.58	Mn2	Os1	12.26	Mn4	Fe1	−1.26	Fe2	Os1	9.14
Mn1	Os1	−12.72	Mn2	Os2	25.43	Mn4	Fe2	−13.27	Fe2	Os2	−33.49
Mn1	Os2	−27.35	Mn3	Mn4	28.61	Mn4	Os1	17.05	Os1	Os2	−6.61

An obvious value of intensity is shown at AFM order wave vector $\boldsymbol{Q}_{\mathrm{AFM}}$ = (0, 0, 1). As the NN interactions are on the order of 10 meV, the maximum of the magnon dispersion reaches 600 meV. Interestingly, the 8 bands along the *Z*−*D* momentum path all show characteristics of flat band.

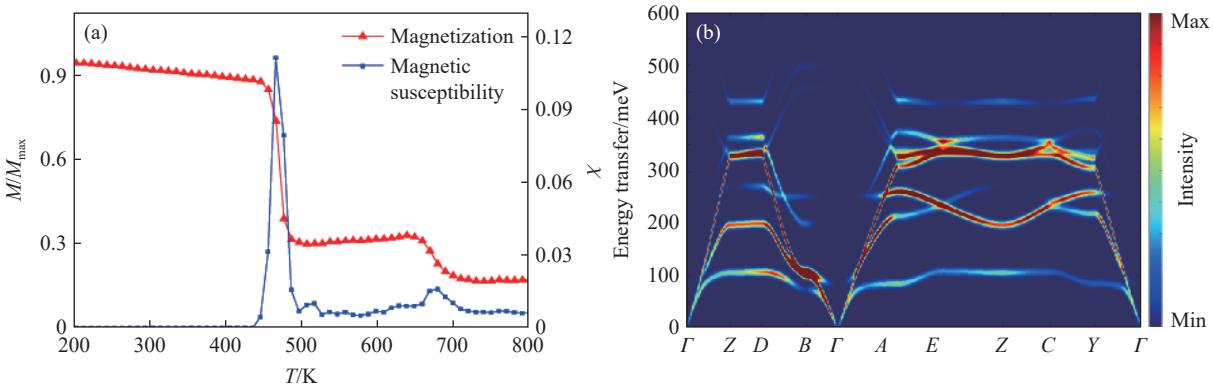


Fig. 4　Magnetism of Mn_2FeOsO_6: (a) calculated magnetization and magnetic susceptibility via classical Monte Carlo simulation (The red line represents the theoretical total magnetic moment M divided by saturation magnetic moment M_{max}, while the blue line represents the relative magnetic susceptibility χ, both indicating the phase transition positions around temparature T about 480 K.); (b) simulated excitation spectrum using SpinW package (The vertical axis represents the energy of the excitation spectrum, and the colors correspond to the intensity of the excitation spectrum.)

In Fig. 4(a), the magnetization and magnetic susceptibility of Mn_2FeOsO_6 were calculated using classical Monte Carlo simulations with Metropolis algorithm. It was observed that the magnetic susceptibility curve has two peaks, indicating the possible existence of two different AFM T_N in this system, consistent with previous experiments[29]. We propose that this phenomenon is due to two sets of AFM atoms at A and B sub-lattices. The higher AFM T_N is directly dependent on the Mn ion at A-sites. The estimated T_N is above 680 K, which is higher than the T_N (or T_C) observed in related experiments. It is noteworthy that the estimated transition temperature is relatively conservative. The actual transition temperature would be further increased if the MAE resulting from shape and DM interaction is considered.

Additionally, the electronic band structure of Mn_2FeOsO_6 was computed, shown in Fig. 3(b). Due to the low lattice symmetry, the energy bands are complex and disordered. However, in contrast to other TMO double perovskites, Mn_2FeOsO_6 exhibits metallic properties, with a high DOS near the Fermi surface. The DOS indicates that the energy band near the Fermi level is primarily contributed by the 3*d* electrons of the magnetic ions. Furthermore, the system presents an AFM configuration, where the spin up and down DOS are consistent, and the total magnetization equals zero. Thus, Mn_2FeOsO_6 is an ideal AFM metallic material.

Finally, the excitation spectrum mode of the above spin model was computed using the spin-wave method. The excitation mode, shown in Fig. 4(b), reveal clear AFM imprints in the <100> direction, consisting of two sets of different AFM excitation spectra, supporting the previously estimated AFM configuration obtained by our Monte Carlo method.

5　Conclusions

In conclusion, we extend a method that can determine the complex magnetism configuration and synthesis condition of double perovskite materials at the same time consuming relatively low computational resources. Our method is shown to provide satisfactory results for several known double perovskite compounds.

We apply this method to investigate the promising material Mn_2FeOsO_6, which has not yet been experimentally synthesized. Our analysis reveals that this material has a $P2_1/n$ structural configuration with a high

density of states near the Fermi level, making it an ideal AFM metal with a total magnetic moment of zero. Using a set of matrix operations, we are able to obtain the complex magnetic exchange interaction of the $P2_1/n$ structure, and identify two sets of AFM T_N. Our findings are further verified by classical Monte Carlo simulations and spin wave excitation spectrum analysis.

Overall, we theoretically identify an ideal AFM metal with extremely high AFM T_N, which has promising applications in the field of spintronics. Our method is an effective approach to study complex magnetism in double perovskite materials and can be extended to investigate other related materials.

References:

[1] FUSIL S, GARCIA V, BARTHÉLÉMY A, et al. Magnetoelectric devices for spintronics [J]. Annual Review of Materials Research, 2014, 44: 91–116.

[2] KOBAYASHI K I, KIMURA T, SAWADA H, et al. Room-temperature magnetoresistance in an oxide material with an ordered double-perovskite structure [J]. Nature, 1998, 395(6703): 677–680.

[3] ZHOU J P, DASS R, YIN H Q, et al. Enhancement of room temperature magnetoresistance in double perovskite ferrimagnets [J]. Journal of Applied Physics, 2000, 87(9): 5037–5039.

[4] SERRAT D, DE TERESA J M, IBARRA M R. Double perovskites with ferromagnetism above room temperature [J]. Journal of Physics: Condensed Matter, 2007, 19(2): 023201.

[5] MORROW R, MISHRA R, RESTREPO O D, et al. Independent ordering of two interpenetrating magnetic sublattices in the double perovskite Sr_2CoOsO_6 [J]. Journal of the American Chemical Society, 2013, 135(50): 18824–18830.

[6] FENG H L, ARAI M, MATSUSHITA Y, et al. High-temperature ferrimagnetism driven by lattice distortion in double perovskite Ca_2FeOsO_6 [J]. Journal of the American Chemical Society, 2014, 136(9): 3326–3329.

[7] CHEN J, WANG X, HU Z W, et al. Enhanced magnetization of the highest-T_C ferrimagnetic oxide Sr_2CrOsO_6 [J]. Physical Review B, 2020, 102(18): 184418.

[8] KROCKENBERGER Y, MOGARE K, REEHUIS M, et al. Sr_2CrOsO_6: end point of a spin-polarized metal-insulator transition by 5*d* band filling [J]. Physical Review B, 2007, 75(2): 020404.

[9] WAKABAYASHI Y K, KROCKENBERGER Y, TSUJIMOTO N, et al. Ferromagnetism above 1 000 K in a highly cation-ordered double-perovskite insulator Sr_3OsO_6 [J]. Nature Communications, 2019, 10(1): 535.

[10] LI R J, ZHU X Z, FU Q F, et al. Nanosheet-based $Nb_{12}O_{29}$ hierarchical microspheres for enhanced lithium storage [J]. Chemical Communications, 2019, 55(17): 2493–2496.

[11] MCCALL S, CAO G, CROW J E, et al. Metamagnetism of single crystal $Ca_3Ru_2O_7$ in high magnetic fields [J]. Physica B: Condensed Matter, 1998, 246/247: 144–148.

[12] KOMAREK A C, STRELTSOV S V, ISOBE M, et al. $CaCrO_3$: an anomalous antiferromagnetic metallic oxide [J]. Physical Review Letters, 2008, 101(16): 167204.

[13] WANG B X, ROSENKRANZ S, RUI X, et al. Antiferromagnetic defect structure in $LaNiO_{3-\delta}$ single crystals [J]. Physical Review Materials, 2018, 2(6): 064404.

[14] LI M R, RETUERTO M, WALKER D, et al. Magnetic-structure-stabilized polarization in an above-room-temperature ferrimagnet [J]. Angewandte Chemie International Edition, 2014, 53(40): 10774–10778.

[15] LI M R, MCCABE E E, STEPHENS P W, et al. Magnetostriction-polarization coupling in multiferroic Mn_2MnWO_6 [J]. Nature Communications, 2017, 8(1): 2037.

[16] LI M R, RETUERTO M, DENG Z, et al. Giant magnetoresistance in the half-metallic double-perovskite ferrimagnet Mn_2FeReO_6 [J]. Angewandte Chemie, 2015, 127(41): 12237–12241.

[17] LI M R, RETUERTO M, STEPHENS P W, et al. Low-temperature cationic rearrangement in a bulk metal oxide [J]. Angewandte Chemie International Edition, 2016, 55(34): 9862–9867.

[18] MORROW R, SOLIZ J R, HAUSER A J, et al. The effect of chemical pressure on the structure and properties of A_2CrOsO_6 (A = Sr, Ca) ferrimagnetic double perovskite [J]. Journal of Solid State Chemistry, 2016, 238: 46–52.

[19] HOU Y S, XIANG H J, GONG X G. Lattice-distortion induced magnetic transition from low-temperature antiferromagnetism

to high-temperature ferrimagnetism in double perovskites A_2FeOsO_6 (A = Ca, Sr) [J]. Scientific Reports, 2015, 5(1): 13159.

[20] NAVEEN K, REEHUIS M, ADLER P, et al. Reentrant magnetism at the borderline between long-range antiferromagnetic order and spin-glass behavior in the B-site disordered perovskite system $Ca_{2-x}Sr_xFeRuO_6$ [J]. Physical Review B, 2018, 98(22): 224423.

[21] ANDERSON M T, GREENWOOD K B, TAYLOR G A, et al. B-cation arrangements in double perovskites [J]. Progress in Solid State Chemistry, 1993, 22(3): 197–233.

[22] GIBB T C. A study of superexchange interactions in the perovskite Sr_2FeRuO_6 by Monte Carlo analysis [J]. Journal of Materials Chemistry, 2005, 15(37): 4015–4019.

[23] CHANG J, LEE K, JUNG M H, et al. Emergence of room-temperature magnetic ordering in artificially fabricated ordered-double-perovskite Sr_2FeRuO_6 [J]. Chemistry of Materials, 2011, 23(11): 2693–2696.

[24] LI M R, CROFT M, STEPHENS P W, et al. Mn_2FeWO_6: a new Ni_3TeO_6-type polar and magnetic oxide [J]. Advanced Materials, 2015, 27(13): 2177–2181.

[25] TAN X Y, MCCABE E E, ORLANDI F, et al. $MnFe_{0.5}Ru_{0.5}O_3$: an above-room-temperature antiferromagnetic semiconductor [J]. Journal of Materials Chemistry C, 2019, 7(3): 509–522.

[26] FRANK C E, MCCABE E E, ORLANDI F, et al. Mn_2CoReO_6: a robust multisublattice antiferromagnetic perovskite with small A-site cations [J]. Chemical Communications, 2019, 55(23): 3331–3334.

[27] LI M R, STEPHENS P W, CROFT M, et al. $Mn_2(Fe_{0.8}Mo_{0.2})MoO_6$: a double perovskite with multiple transition metal sublattice magnetic effects [J]. Chemistry of Materials, 2018, 30(14): 4508–4514.

[28] CAI G H, GREENBLATT M, LI M R. Polar magnets in double corundum oxides [J]. Chemistry of Materials, 2017, 29(13): 5447–5457.

[29] LI M R, HODGES J P, RETUERTO M, et al. Mn_2MnReO_6: synthesis and magnetic structure determination of a new transition-metal-only double perovskite canted antiferromagnet [J]. Chemistry of Materials, 2016, 28(9): 3148–3158.

[30] ARÉVALO-LÓPEZ A M, MCNALLY G M, ATTFIELD J P. Large magnetization and frustration switching of magnetoresistance in the double-perovskite ferrimagnet Mn_2FeReO_6 [J]. Angewandte Chemie International Edition, 2015, 54(41): 12074–12077.

[31] ARÉVALO-LÓPEZ A M, STEGEMANN F, ATTFIELD J P. Competing antiferromagnetic orders in the double perovskite Mn_2MnReO_6 (Mn_3ReO_6) [J]. Chemical Communications, 2016, 52(32): 5558–5560.

[32] VASALA S, KARPPINEN M. $A_2B'B''O_6$ perovskites: a review [J]. Progress in Solid State Chemistry, 2015, 43(1/2): 1–36.

[33] GILIOLI E, EHM L. High pressure and multiferroics materials: a happy marriage [J]. IUCrJ, 2014, 1(6): 590–603.

[34] BELIK A A, YI W. High-pressure synthesis, crystal chemistry and physics of perovskites with small cations at the A site [J]. Journal of Physics: Condensed Matter, 2014, 26(16): 163201.

[35] SHANNON R D. Revised effective ionic radii and systematic studies of interatomic distances in halides and chalcogenides [J]. Acta Crystallographica Section A: Crystal Physics, Diffraction, Theoretical and General Crystallography, 1976, 32(5): 751–767.

[36] SCHULZ H, BAYER G. Structure determination of Mg_3TeO_6 [J]. Acta Crystallographica Section B: Structural Crystallography and Crystal Chemistry, 1971, 27(4): 815–821.

[37] SELB E, DECLARA L, BAYARJARGAL L, et al. Crystal structure and properties of a UV-transparent high-pressure polymorph of Mg_3TeO_6 with second harmonic generation response [J]. European Journal of Inorganic Chemistry, 2019, 2019(43): 4668–4676.

[38] GHOSH A, CHEN K H, QIU X S, et al. Anisotropy in the magnetic interaction and lattice-orbital coupling of single crystal Ni_3TeO_6 [J]. Scientific Reports, 2018, 8(1): 15779.

[39] FERNÁNDEZ-CATALÁ J, SINGH H, WANG S B, et al. Hydrothermal synthesis of Ni_3TeO_6 and Cu_3TeO_6 nanostructures for magnetic and photoconductivity applications [J]. ACS Applied Nano Materials, 2023, 6(6): 4887–4897.

[40] HAN Y F, ZENG Y J, HENDRICKX M, et al. Universal A-cation splitting in $LiNbO_3$-type structure driven by intrapositional multivalent coupling [J]. Journal of the American Chemical Society, 2020, 142(15): 7168–7178.

[41] FUJITA K, KAWAMOTO T, YAMADA I, et al. $LiNbO_3$-type $InFeO_3$: room-temperature polar magnet without second-order Jahn-Teller active ions [J]. Chemistry of Materials, 2016, 28(18): 6644–6655.

[42] VARGA T, KUMAR A, VLAHOS E, et al. Coexistence of weak ferromagnetism and ferroelectricity in the high pressure $LiNbO_3$-type phase of $FeTiO_3$ [J]. Physical Review Letters, 2009, 103(4): 047601.

[43] BELIK A A, STEFANOVICH S Y, LAZORYAK B I, et al. $BiInO_3$: a polar oxide with $GdFeO_3$-type perovskite structure [J].

Chemistry of Materials, 2006, 18(7): 1964–1968.

[44] VASYLECHKO L, MATKOVSKII A, SAVYTSKII D, et al. Crystal structure of $GdFeO_3$-type rare earth gallates and aluminates [J]. Journal of Alloys and Compounds, 1999, 291(1/2): 57–65.

[45] MALYI O I, DALPIAN G M, ZHAO X G, et al. Realization of predicted exotic materials: the burden of proof [J]. Materials Today, 2020, 32: 35–45.

[46] LUFASO M W, WOODWARD P M. Prediction of the crystal structures of perovskites using the software program SPuDS [J]. Acta Crystallographica Section B: Structural Science, 2001, 57(6): 725–738.

[47] BARTEL C J, SUTTON C, GOLDSMITH B R, et al. New tolerance factor to predict the stability of perovskite oxides and halides [J]. Science Advances, 2019, 5(2): eaav0693.

[48] FILIP M R, GIUSTINO F. The geometric blueprint of perovskites [J]. Proceedings of the National Academy of Sciences of the United States of America, 2018, 115(21): 5397–5402.

[49] SUN Q D, YIN W J. Thermodynamic stability trend of cubic perovskites [J]. Journal of the American Chemical Society, 2017, 139(42): 14905–14908.

[50] CHEN P, LIU B G. Giant ferroelectric polarization and electric reversal of strong spontaneous magnetization in multiferroic Bi_2FeMoO_6 [J]. Journal of Magnetism and Magnetic Materials, 2017, 441: 497–502.

[51] CHEN P, GRISOLIA M N, ZHAO H J, et al. Energetics of oxygen-octahedra rotations in perovskite oxides from first principles [J]. Physical Review B, 2018, 97(2): 024113.

[52] SU H P, LI S F, HAN Y F, et al. Predicted polymorph manipulation in an exotic double perovskite oxide [J]. Journal of Materials Chemistry C, 2019, 7(39): 12306–12311.

[53] HAN Y F, WU M X, GUI C R, et al. Data-driven computational prediction and experimental realization of exotic perovskite-related polar magnets [J]. NPJ Quantum Materials, 2020, 5(1): 92.

[54] MURNAGHAN F D. The compressibility of media under extreme pressures [J]. Proceedings of the National Academy of Sciences of the United States of America, 1944, 30(9): 244–247.

[55] HALDER A, GHOSH A, DASGUPTA T S. Machine-learning-assisted prediction of magnetic double perovskites [J]. Physical Review Materials, 2019, 3(8): 084418.

[56] HALDER A, NAFDAY D, SANYAL P, et al. Computer predictions on Rh-based double perovskites with unusual electronic and magnetic properties [J]. NPJ Quantum Materials, 2018, 3(1): 17.

[57] ZHAO H J, ÍÑIGUEZ J, REN W, et al. Atomistic theory of hybrid improper ferroelectricity in perovskites [J]. Physical Review B, 2014, 89(17): 174101.

[58] BENEDEK N A, FENNIE C J. Why are there so few perovskite ferroelectrics [J]. The Journal of Physical Chemistry C, 2013, 117(26): 13339–13349.

[59] HOWARD C J, KENNEDY B J, WOODWARD P M. Ordered double perovskites—a group-theoretical analysis [J]. Acta Crystallographica Section B, 2003, 59(4): 463–471.

[60] GLAZER A M. The classification of tilted octahedra in perovskites [J]. Acta Crystallographica Section B, 1972, 28(11): 3384–3392.

[61] RONDINELLI J M, MAY S J, FREELAND J W. Control of octahedral connectivity in perovskite oxide heterostructures: an emerging route to multifunctional materials discovery [J]. MRS Bulletin, 2012, 37(3): 261–270.

[62] ZHOU Q D, TAN T Y, KENNEDY B J, et al. Crystal structures and phase transitions in Sr doped Ba_2InTaO_6 perovskites [J]. Journal of Solid State Chemistry, 2013, 206: 122–128.

[63] FU W T, GÖTZ R J, IJDO D J W. On the symmetry and crystal structures of Ba_2LaIrO_6 [J]. Journal of Solid State Chemistry, 2010, 183(2): 419–424.

[64] GUENNOU M, BOUVIER P, CHEN G S, et al. Multiple high-pressure phase transitions in $BiFeO_3$ [J]. Physical Review B, 2011, 84(17): 174107.

[65] XIE T, GROSSMAN J C. Crystal graph convolutional neural networks for an accurate and interpretable prediction of material properties [J]. Physical Review Letters, 2018, 120(14): 145301.

[66] WANG Y C, MA Y M. Perspective: crystal structure prediction at high pressures [J]. The Journal of Chemical Physics, 2014, 140(4): 040901.

[67] KRESSE G, HAFNER J. *Ab initio* molecular dynamics for liquid metals [J]. Physical Review B, 1993, 47(1): 558–561.

[68] KRESSE G, JOUBERT D. From ultrasoft pseudopotentials to the projector augmented-wave method [J]. Physical Review B,

1999, 59(3): 1758–1775.

[69] KRESSE G, HAFNER J. *Ab initio* molecular-dynamics simulation of the liquid-metal-amorphous-semiconductor transition in germanium [J]. Physical Review B, 1994, 49(20): 14251–14269.

[70] BLÖCHL P E. Projector augmented-wave method [J]. Physical Review B, 1994, 50(24): 17953–17979.

[71] PERDEW J P, BURKE K, ERNZERHOF M. Generalized gradient approximation made simple [J]. Physical Review Letters, 1996, 77(18): 3865–3868.

[72] TOTH S, LAKE B. Linear spin wave theory for single-Q incommensurate magnetic structures [J]. Journal of Physics: Condensed Matter, 2015, 27(16): 166002.

[73] SOLANA-MADRUGA E, ALHARBI, K N, HERZ M, et al. Unconventional magnetism in the high pressure ‘all transition metal’ double perovskite Mn_2NiReO_6 [J]. Chemical Communications, 2020, 56(83): 12574–12577.

[74] LI S D, CHEN P, LIU B G. Promising ferrimagnetic double perovskite oxides towards high spin polarization at high temperature [J]. AIP Advances, 2013, 3(1): 012107.

双钙钛矿反铁磁体 Mn_2FeOsO_6 的合成条件和磁性性质的理论预测

李　军[1], 金尚健[2], 赵　爽[3], 姚道新[2], 李满荣[3,4]

（1. 燕山大学理学院, 河北省微结构材料物理重点实验室, 河北 秦皇岛　066004;
2. 中山大学物理学院, 光电材料与技术国家重点实验室, 广东 广州　510275;
3. 中山大学化学学院, 生物无机与合成化学教育部重点实验室, 广东 广州　510275;
4. 海南大学理学院, 海南 海口　570228）

摘要: 提出了一种理论方法, 用于预测复杂磁性双钙钛矿化合物的电子构型、多晶体形态、合成条件和物理性质。该方法对于双钙钛矿化合物的预测准确且高效。确定了一种反铁磁金属材料 Mn_2FeOsO_6, 它具有极高的反铁磁 Néel 相变温度（T_N）。大量分析表明 Mn_2FeOsO_6 在费米能级附近具有很高的态密度和反铁磁构型, 总磁矩为零。本研究结果表明, Mn_2FeOsO_6 的 T_N 高达 680 K, 代表自旋电子学领域的一个潜在突破。构建了 Mn_2FeOsO_6 的 T_N 的复杂磁性模型, 获得了相对可靠的磁激发谱, 可与潜在的中子散射谱进行比较。这一理论方法得到的合成条件符合许多已合成的双钙钛矿化合物的实验合成条件, 且该方法具有预测其他复杂磁性构型的潜力。研究成果有望在新型双钙钛矿材料的大数据预测中发挥关键作用。

关键词: 双钙钛矿; 反铁磁体; Mn_2FeOsO_6

中图分类号: O521.2　　**文献标志码:** A